*Supporting Information for*

# Hydrozone-based Cobalt Complexes Toward Multielectron Redox and Spin Crossover

Wei Huang, Yujie Li, Juan Yong, Yang Liu and Dayu Wu*

Jiangsu Key Laboratory of Advanced Catalytic Materials and Technology, Collaborative Innovation Center of Advanced Catalysis & Green Manufacturing, School of Petrochemical Engineering, Changzhou University, Changzhou, Jiangsu 213164, China.

Email: wudy@cczu.edu.cn.

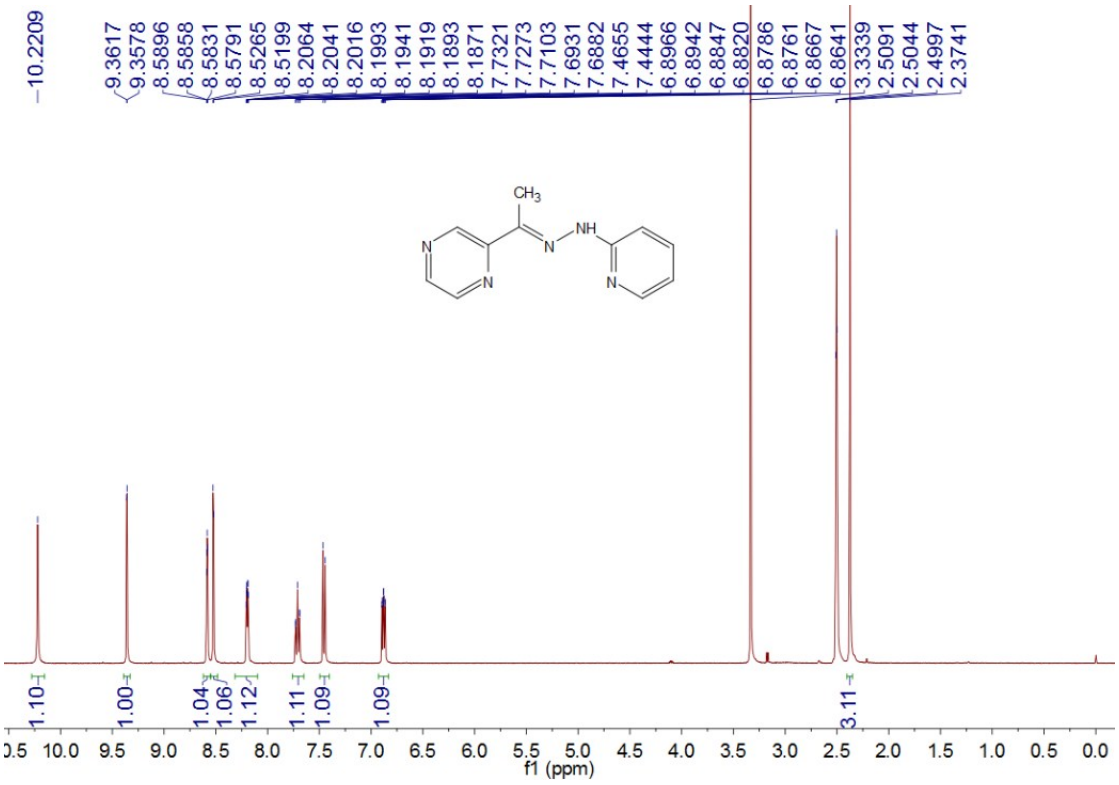


**Fig. S1**. $^{1}$H-NMR spectra of **HL1** (DMSO-d$^{6}$)

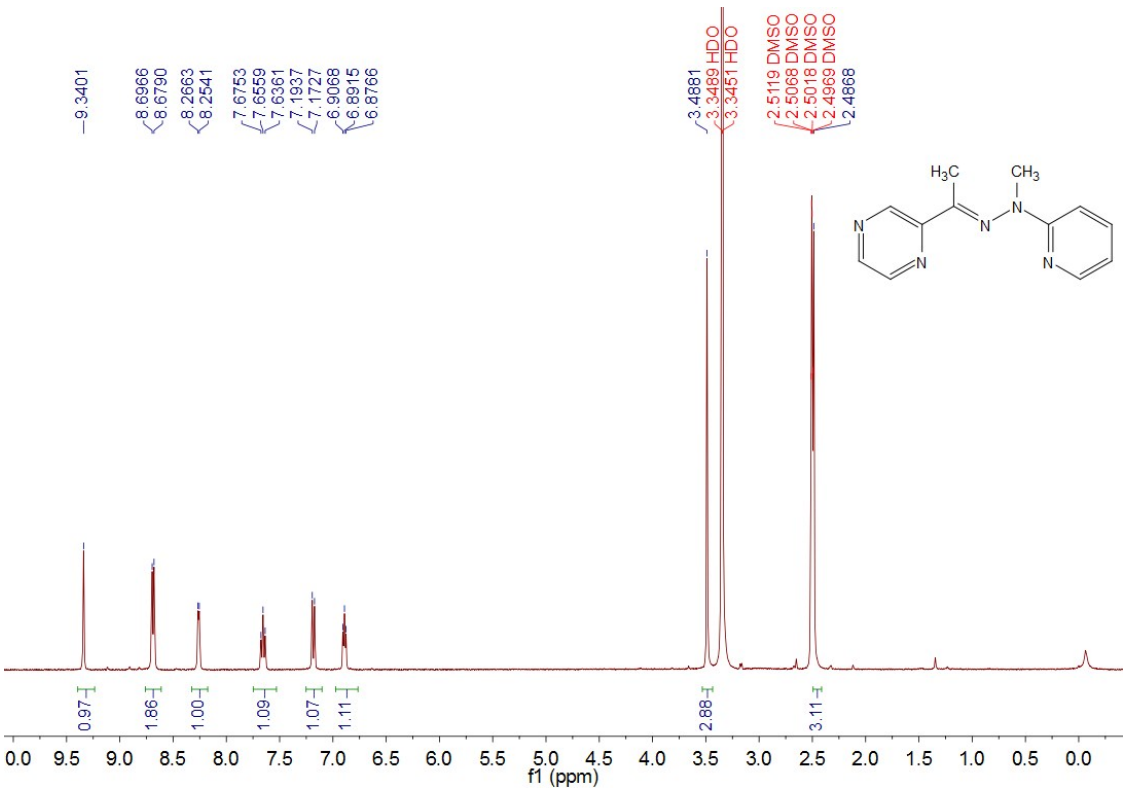


**Fig. S2**. $^{1}$H-NMR spectra of **L2$^{Me}$** (DMSO-d$^{6}$)

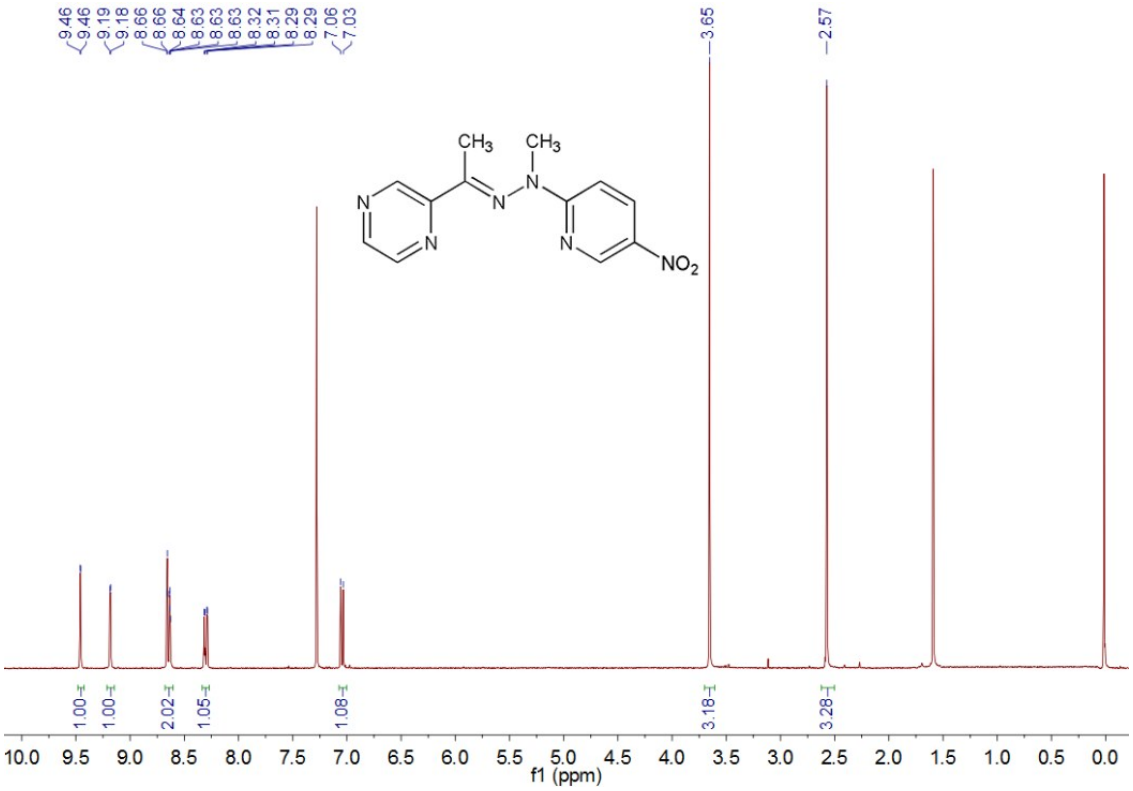


**Fig. S3**. $^{1}$H-NMR spectra of **L3$^{NO2}$** ($CDCl_3$)

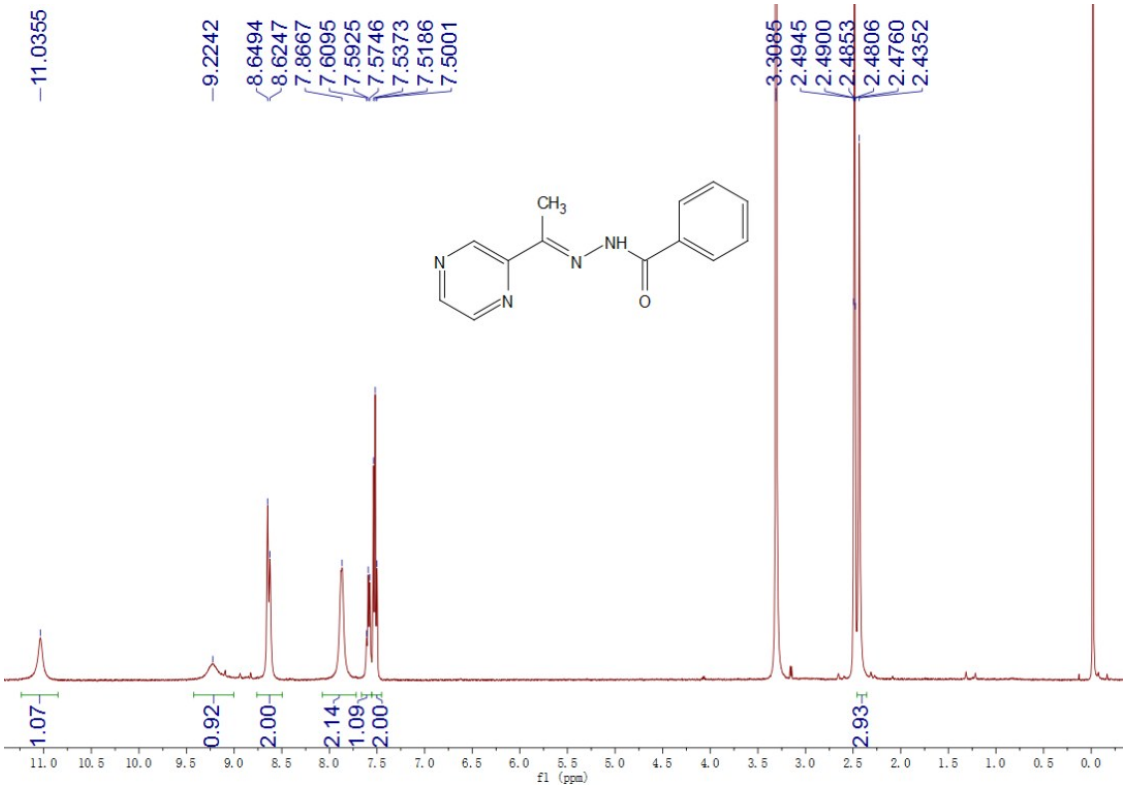


**Fig. S4**. $^{1}$H-NMR spectra of **HL4** (DMSO-d$^{6}$).

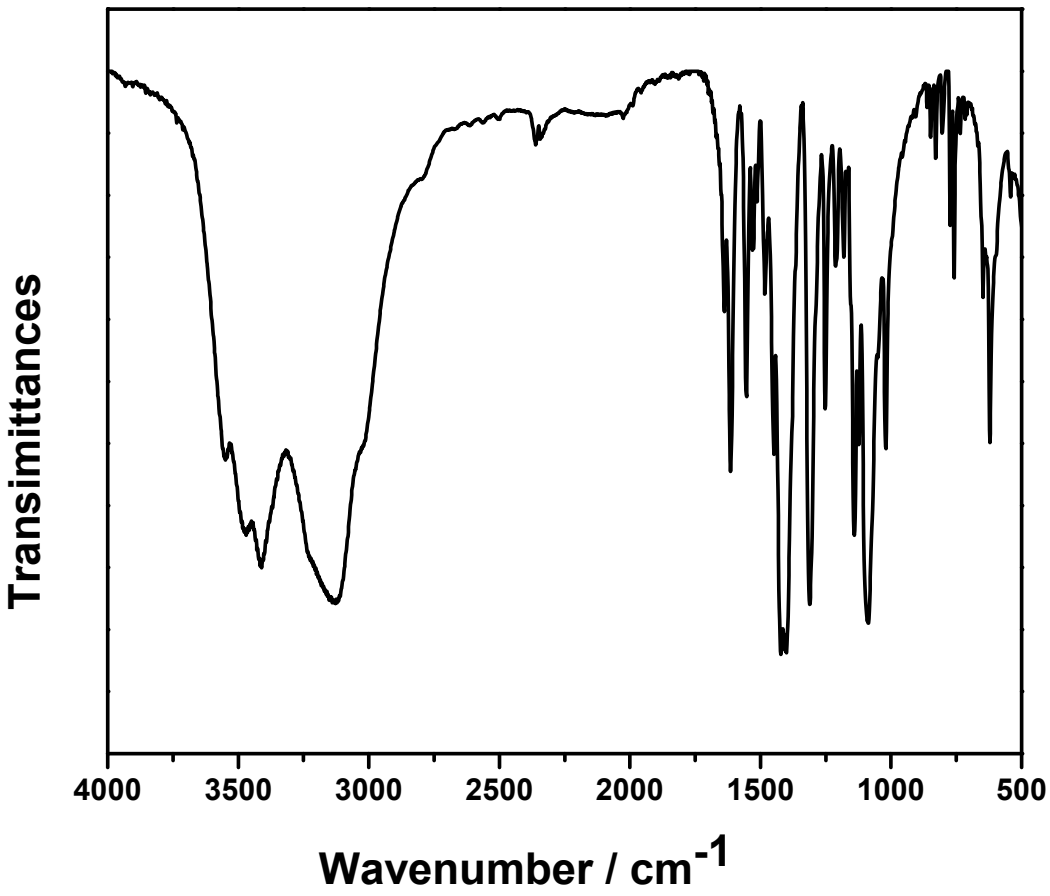


**Fig. S5**.IR spectrum of complex **1.**

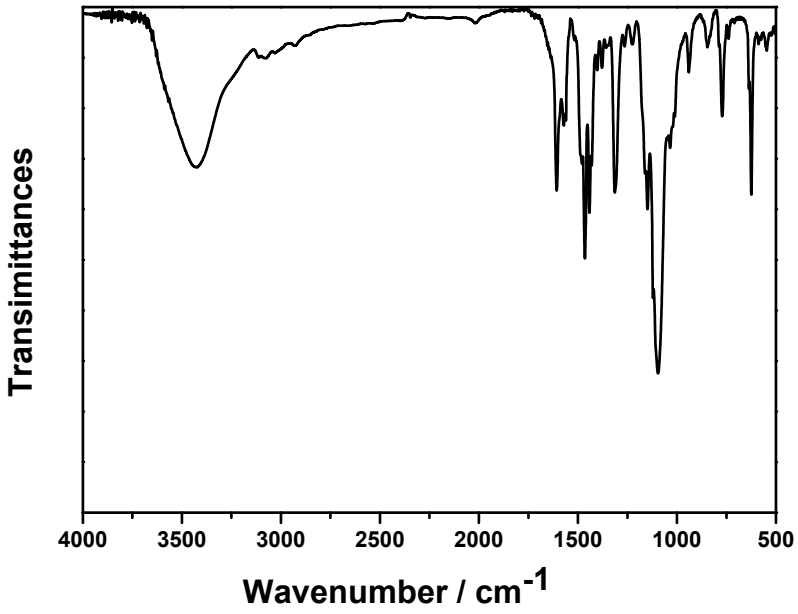


**Fig. S6**.IR spectrum of complex **2.**

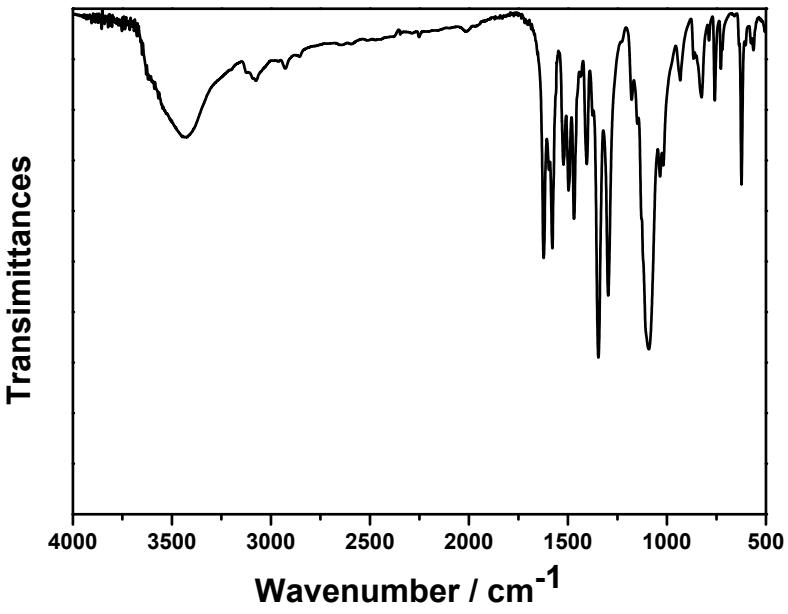


**Fig. S7**. IR spectrum of complex $\mathbf{3_{ClO4}\cdot CH_3OH}$.

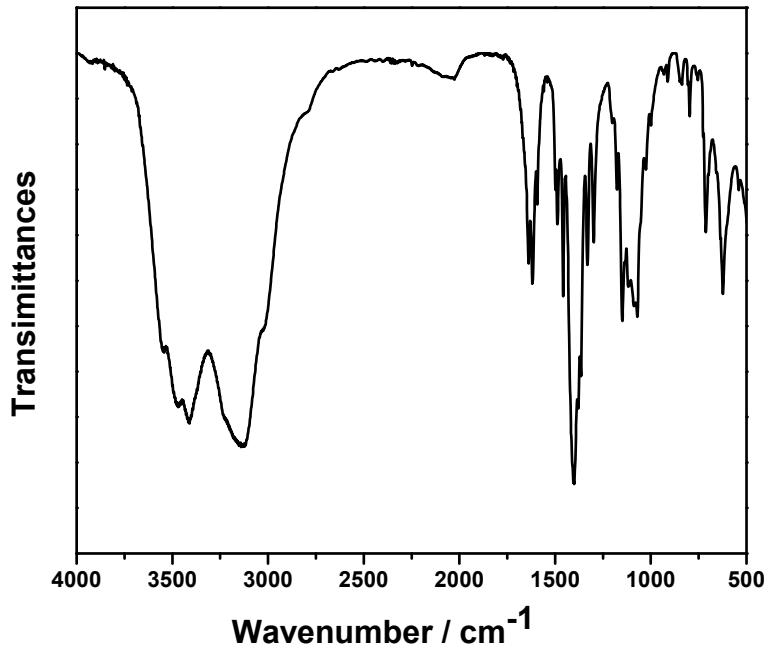


**Fig. S8**.IR spectrum of complex **4.**

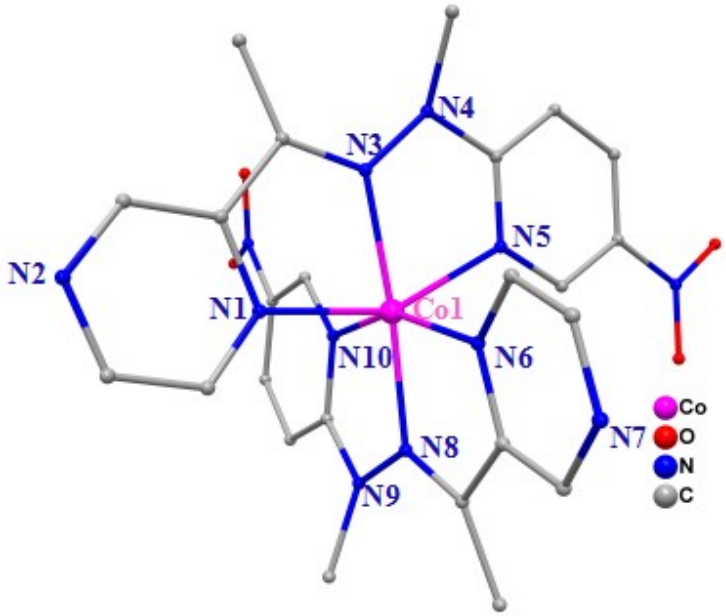


**Fig. S9**. Crystal structure of the compound $3_{BF4}\cdot 0.5CH_3OH$.

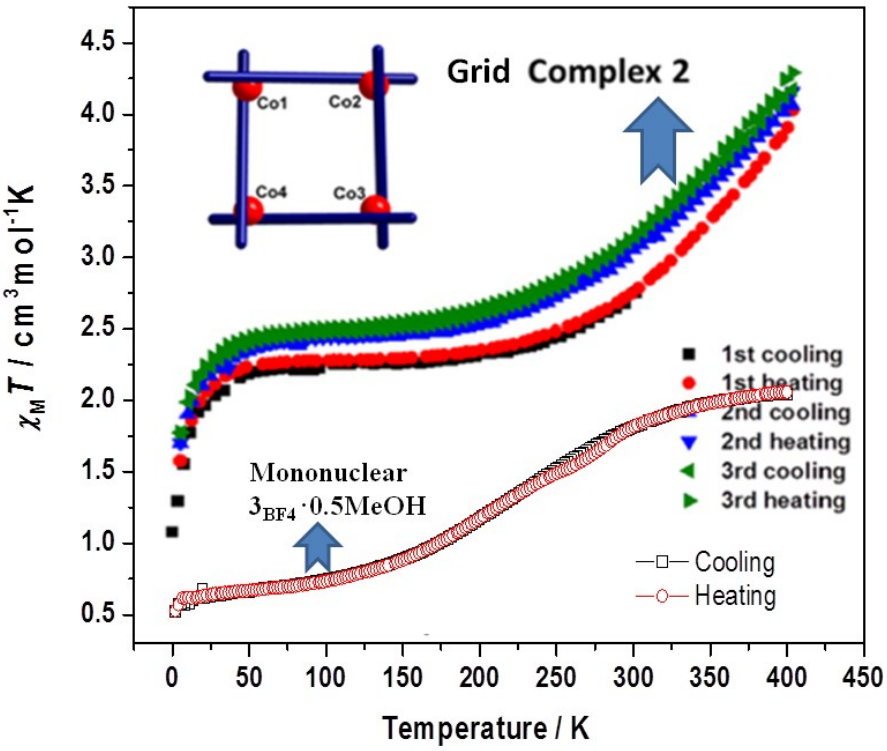


**Fig. S10**. The combined plot of magnetic data for mononuclear compound $\mathbf{3}_{\mathbf{BF4}}$ and the reported tetranuclear grid complex.

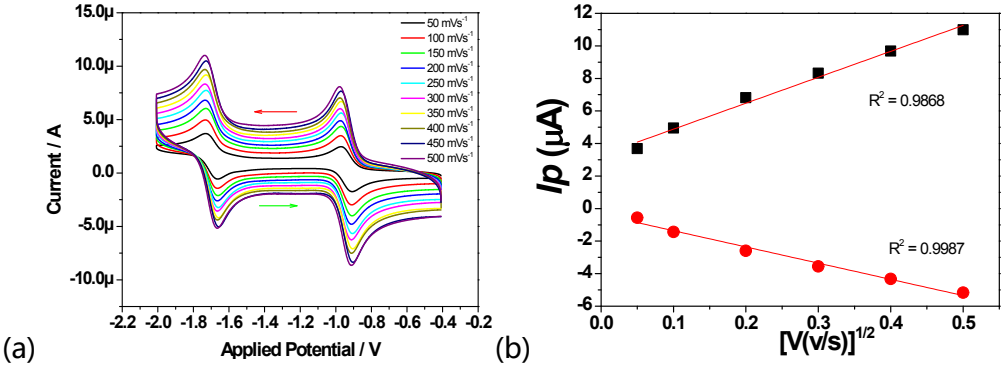


**Fig. S11**.(a)CV study of an acetonitrile solution of complex **1** (0.1 mM) referenced against $Fc^{+}/Fc$. (b) Plots of anodic and cathodic peak currents at redox process II versus the square root of the scan rates, $v^{1/2}$.

Table S1. Summary of Electrochemical Data for Cobalt(III) complex **1**.

| Scan rate($mVs^{-1}$) | $Co^{3+/2+}$ | | | | $Co^{2+/+}$ | | | |
|---|---|---|---|---|---|---|---|---|
| | $E_{ox}$ (v) | $E_{red}$ (v) | ΔE | $E_m$ (v) | $E_{ox}$ (v) | $E_{red}$ (v) | ΔE | $E_m$ (v) |
| 50 | -0.905 | -0.965 | 0.060 | -0.935 | -1.667 | -1.732 | 0.065 | -1.699 |
| 100 | -0.923 | -0.974 | 0.051 | -0.948 | -1.672 | -1.741 | 0.069 | -1.706 |
| 150 | -0.926 | -0.983 | 0.057 | -0.954 | -1.676 | -1.746 | 0.070 | -1.711 |
| 200 | -0.931 | -0.985 | 0.054 | -0.958 | -1.676 | -1.746 | 0.070 | -1.711 |
| 250 | -0.934 | -0.989 | 0.055 | -0.962 | -1.682 | -1.745 | 0.063 | -1.714 |
| 300 | -0.936 | -0.992 | 0.056 | -0.964 | -1.668 | -1.744 | 0.076 | -1.706 |
| 350 | -0.940 | -0.981 | 0.041 | -0.960 | -1.671 | -1.745 | 0.074 | -1.708 |
| 400 | -0.942 | -0.986 | 0.044 | -0.964 | -1.672 | -1.748 | 0.076 | -1.710 |
| 450 | -0.943 | -0.987 | 0.044 | -0.965 | -1.678 | -1.739 | 0.061 | -1.708 |
| 500 | -0.948 | -0.989 | 0.041 | -0.968 | -1.673 | -1.742 | 0.069 | -1.708 |

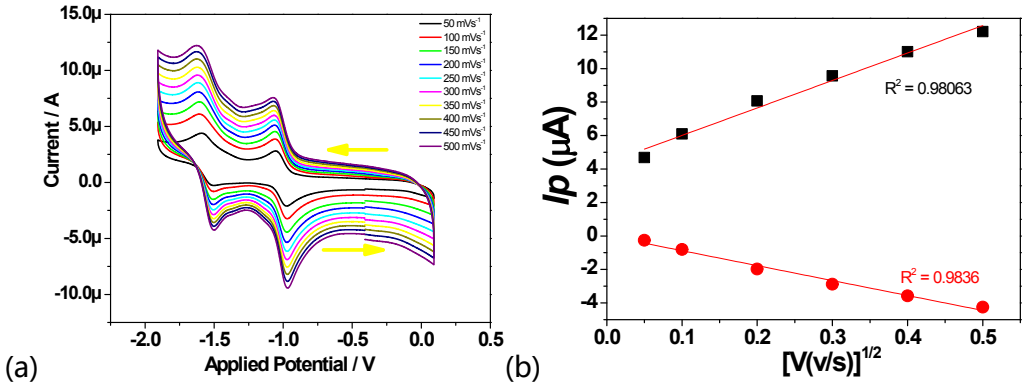


**Fig. S12**. (a) CV study of an acetonitrile solution of complex **2** (0.1 mM) referenced against $Fc^{+}/Fc$. (b) Plots of anodic and cathodic peak currents at redox process II versus the square root of the scan rates, $v^{1/2}$.

Table S2. Summary of Electrochemical Data for Cobalt(III) complex **2**.

| Scan rate($mVs^{-1}$) | $Co^{3+/2+}$ | | | | $Co^{2+/+}$ | | | |
|---|---|---|---|---|---|---|---|---|
| | $E_{ox}$ (v) | $E_{red}$ (v) | ΔE | $E_m$ (v) | $E_{ox}$ (v) | $E_{red}$ (v) | ΔE | $E_m$ (v) |
| 50 | -0.976 | -1.061 | 0.085 | -1.018 | -1.520 | -1.594 | 0.074 | -1.557 |
| 100 | -0.971 | -1.062 | 0.091 | -1.016 | -1.502 | -1.607 | 0.105 | -1.554 |
| 150 | -0.971 | -1.064 | 0.093 | -1.018 | -1.504 | -1.609 | 0.105 | -1.556 |
| 200 | -0.970 | -1.066 | 0.096 | -1.018 | -1.503 | -1.611 | 0.108 | -1.557 |
| 250 | -0.969 | -1.065 | 0.096 | -1.017 | -1.502 | -1.619 | 0.117 | -1.560 |
| 300 | -0.967 | -1.066 | 0.099 | -1.016 | -1.501 | -1.620 | 0.119 | -1.560 |
| 350 | -0.965 | -1.067 | 0.102 | -1.016 | -1.500 | -1.622 | 0.122 | -1.561 |
| 400 | -0.964 | -1.068 | 0.104 | -1.016 | -1.500 | -1.623 | 0.123 | -1.562 |
| 450 | -0.964 | -1.070 | 0.106 | -1.017 | -1.499 | -1.628 | 0.129 | -1.564 |
| 500 | -0.964 | -1.071 | 0.107 | -1.018 | -1.498 | -1.629 | 0.131 | -1.564 |

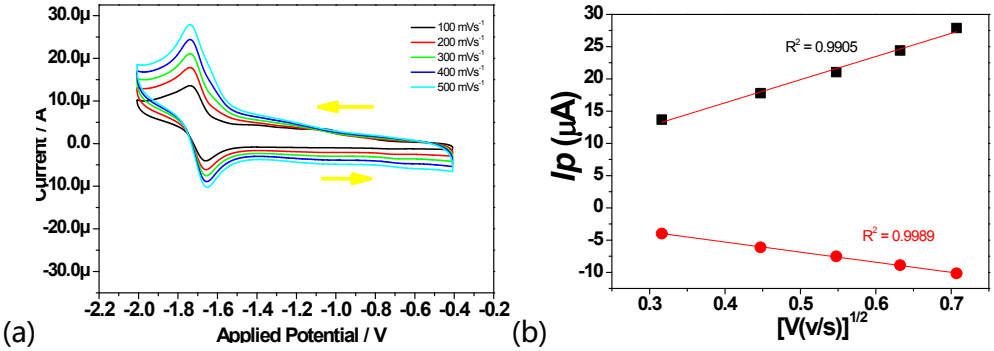


**Fig. S13**. (a) CV study of an acetonitrile solution of Complex $\mathbf{3}_{\mathbf{ClO4}}$ (0.1 mM) referenced against $Fc^{+}/Fc$. (b) Plots of anodic and cathodic peak currents at redox process II versus the square root of the scan rates, $v^{1/2}$.

Table S3. Summary of Electrochemical Data for Cobalt(III) complex $\mathbf{3}_{\mathbf{ClO4}}$.

| Scan rate($mVs^{-1}$) | $Co^{2+/+}$ | | | |
|---|---|---|---|---|
| | $E_{ox}$ (v) | $E_{red}$ (v) | ΔE | $E_m$ (v) |
| 100 | -1.660 | -1.738 | 0.078 | -1.699 |
| 200 | -1.657 | -1.739 | 0.082 | -1.698 |
| 300 | -1.653 | -1.739 | 0.086 | -1.696 |
| 400 | -1.652 | -1.740 | 0.088 | -1.696 |
| 500 | -1.651 | -1.740 | 0.089 | -1.696 |

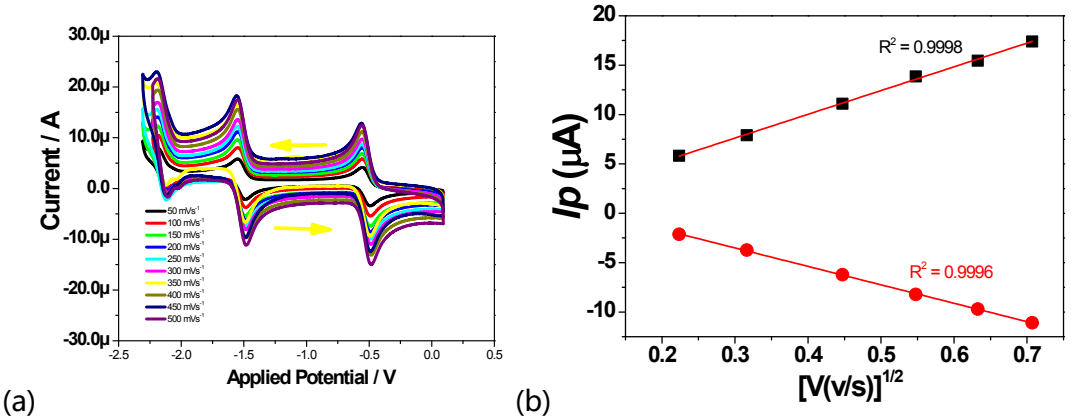


**Fig. S14**. (a) CV study of an acetonitrile solution of complex **4** (0.1 mM) referenced against $Fc^{+}/Fc$. (b) Plots of anodic and cathodic peak currents at redox process II versus the square root of the scan rates, $v^{1/2}$.

Table S4. Summary of Electrochemical Data for Cobalt(III) complex **4**.

| Scan rate($mVs^{-1}$) | $Co^{3+/2+}$ | | | | $Co^{2+/+}$ | | | | Ligand-base | | | |
|---|---|---|---|---|---|---|---|---|---|---|---|---|
| | $E_{red}$ (v) | $E_{ox}$ (v) | ΔE | $E_m$ (v) | $E_{red}$ (v) | $E_{ox}$ (v) | ΔE | $E_m$ (v) | $E_{red}$ (v) | $E_{ox}$ (v) | ΔE | $E_m$ (v) |
| 50 | -0.555 | -0.490 | -0.065 | -0.522 | -1.548 | -1.486 | -0.062 | -1.517 | -2.185 | -2.115 | -0.070 | -2.150 |
| 100 | -0.557 | -0.489 | -0.068 | -0.523 | -1.546 | -1.484 | -0.062 | -1.515 | -2.192 | -2.112 | -0.080 | -2.152 |
| 150 | -0.559 | -0.489 | -0.070 | -0.524 | -1.550 | -1.486 | -0.064 | -1.518 | -2.194 | -2.113 | -0.081 | -2.158 |
| 200 | -0.553 | -0.487 | -0.066 | -0.520 | -1.548 | -1.484 | -0.064 | -1.516 | -2.185 | -2.115 | -0.070 | -2.150 |
| 250 | -0.558 | -0.486 | -0.072 | -0.522 | -1.554 | -1.483 | -0.071 | -1.518 | -2.187 | -2.117 | -0.070 | -2.152 |
| 300 | -0.558 | -0.487 | -0.071 | -0.522 | -1.552 | -1.482 | -0.070 | -1.517 | -2.188 | -2.113 | -0.075 | -2.150 |
| 350 | -0.559 | -0.485 | -0.074 | -0.522 | -1.557 | -1.481 | -0.076 | -1.519 | -2.192 | -2.119 | -0.073 | -2.156 |
| 400 | -0.560 | -0.486 | -0.074 | -0.523 | -1.553 | -1.480 | -0.073 | -1.516 | -2.188 | -2.116 | -0.072 | -2.152 |
| 450 | -0.562 | -0.484 | -0.078 | -0.523 | -1.558 | -1.480 | -0.078 | -1.519 | -2.195 | -2.107 | -0.088 | -2.151 |
| 500 | -0.560 | -0.484 | -0.076 | -0.522 | -1.554 | -1.479 | -0.075 | -1.516 | -2.191 | -2.104 | -0.087 | -2.148 |